very good when the displaced atoms are nearest neighbors to each other. Including interference terms need not, of course, necessarily reduce the scattering, and may, when treated in detail, even lead to an enhancement of $\Delta\rho_D$.

(3) The results of J would indicate that $|m|^2$ and $|M|^2$, in the notation of Dexter,[16] are, in arbitrary units, of order 1.5 and 3.5, respectively. Now it was shown in reference 16 that the matrix elements m and M are, in the case of interstitials, very likely of opposite sign. Since the resistivity is in fact related to $|m+M|^2$, the above values for $|m|^2$ and $|M|^2$ may well lead to a rather small resistivity change due to interstitials, perhaps of order 0.5 μohm-cm/atomic percent. This crude argument is used here only to point out that it is essential to include interference effects when scattering from the imperfection and from the associated lattice distortion appears to be of the same magnitude when considered independently. [See also D. L. Dexter, Phys. Rev. **98**, 543 (1955).]

PHYSICAL REVIEW VOLUME 99, NUMBER 6 SEPTEMBER 15, 1955

de Haas-van Alphen Effect in Arsenic

TED G. BERLINCOURT
United States Naval Research Laboratory, Washington, D. C.
(Received March 24, 1955)

The de Haas-van Alphen effect has been studied in single crystals of rhombohedral (metallic) arsenic in the liquid helium temperature range and in magnetic fields up to 25 kilogauss. The effect in arsenic is characterized by long-period (up to $\sim 4\times10^{-5}$ gauss^{-1}) oscillations upon which are superposed three short period (up to $\sim 6\times10^{-7}$ gauss^{-1}) terms. Analysis in terms of existing theory attributes the long-period oscillations to electrons occupying a constant energy surface in momentum or wave-number space which to a first approximation is an ellipsoid of revolution with a degeneracy energy $E_{0l}=1.59\times10^{-14}$ erg. The pertinent electrons in the case of the short-period oscillations can be attributed to three identical ellipsoidal constant-energy surfaces oriented so as to satisfy the trigonal symmetry of the arsenic lattice and having a degeneracy energy $E_{0s}=29.4\times10^{-14}$ erg. In addition, the electronic effective masses have been evaluated.
A method for growing arsenic single crystals is described.

INTRODUCTION AND THEORY

THE de Haas-van Alphen effect is characterized by a periodic dependence of the magnetic susceptibility of metal single crystals upon reciprocal magnetic field at low temperatures. Since its discovery by de Haas and van Alphen[1] in bismuth, the effect has been observed in fourteen other metal single crystals,[2] and correlations have been established between the susceptibility oscillations and similar oscillations in the magnetoresistance,[3–5] Hall effect,[6,7] thermoelectric effect,[8] and thermal conductivity.[9]

The discovery of short-period susceptibility oscillations in arsenic was reported briefly in an earlier communication[10] by the author. In addition, much-longer-period oscillations have subsequently been detected, and the present paper concerns detailed investigations of both the long- and short-period terms.

The theory of the de Haas-van Alphen effect was developed by Peierls,[11] Blackman,[12] and Landau[13] and is based upon a free-electron model. In the presence of a magnetic field the electronic energy levels coalesce into quantized levels of field-dependent spacing and degeneracy. As the field is varied, the electrons are redistributed among these levels in such a way as to give rise to the susceptibility oscillations. The effect of the periodic electric field of the lattice is taken into account by the introduction of anistropic effective electronic masses, and in many cases (including arsenic) the pertinent constant-energy surfaces in momentum or wave-number space may be approximated by one or more ellipsoids. Such approximately ellipsoidal pockets of electrons (or holes) presumably exist where the Fermi surface overlaps (or underlaps) Brillouin zone boundaries. The resulting high curvature and correspondingly low degeneracy energy and low effective electronic masses favor easy detection of the de Haas-van Alphen effect.

Equation (1), obtained from Landau's theory (see

[1] W. J. de Haas and P. M. van Alphen, Leiden Comm. No. 212 A (1930).
[2] D. Shoenberg, Trans. Roy. Soc. (London) **245**, 1 (1952). This reference discusses most of the work before 1952.
[3] P. B. Alers and R. T. Webber, Phys. Rev. **91**, 1060 (1953).
[4] Ted G. Berlincourt, Phys. Rev. **91**, 1277 (1953).
[5] T. G. Berlincourt and J. K. Logan, Phys. Rev. **93**, 348 (1954).
[6] Laird C. Brodie, Phys. Rev. **93**, 935 (1954).
[7] Reynolds, Leinhardt, and Hemstreet, Phys. Rev. **93**, 247 (1954).
[8] M. C. Steele and J. Babiskin, Phys. Rev. **94**, 1394 (1954).
[9] J. Babiskin and M. C. Steele, Phys. Rev. **96**, 822 (1954). Also, P. B. Alers, Phys. Rev. **98**, 1180(A) (1955).
[10] Ted G. Berlincourt, Phys. Rev. **92**, 1068 (1953).
[11] R. Peierls, Z. Physik **81**, 186 (1933).
[12] M. Blackman, Proc. Roy. Soc. (London) **A166**, 1 (1938).
[13] L. D. Landau, see Appendix of D. Shoenberg, Proc. Roy. Soc. (London) **A170**, 341 (1939).

reference 2), gives the difference between the magnetic susceptipilities ($\Delta\chi$) per unit mass in two directions at right angles to each other for the case of ellipsoidal constant energy surfaces. (Recent modifications of this theory and methods for evaluating electronic parameters from the experimental data will be discussed later.)

$$\Delta\chi=\sum\frac{A\Delta m}{\rho}\left\{\frac{\pi^2}{6}\left(\frac{k}{E_0}\right)^{\frac{1}{2}}-\frac{1}{T^{\frac{1}{2}}}\left(\frac{2\pi^2kT}{\beta H}\right)^{\frac{3}{2}}\times\sum_{p=1}^{\infty}\frac{(-1)^{p+1}\sin(2\pi pE_0/\beta H-\pi/4)}{2p^{\frac{1}{2}}\sinh(2\pi^2pkT/\beta H)}\right\},\quad(1)$$

provided $E_0\gg kT$ and $E_0\gg\beta H$. As will be evident later, the latter is not fulfilled for the long period oscillations at the highest fields of this investigation. A is a constant given by

$$A\equiv\frac{e^2E_0}{\pi^4c^2\hbar(2k)^{\frac{1}{2}}(m')^{\frac{3}{2}}},\quad(2)$$

ρ is the density, β is a double effective Bohr magneton given by

$$\beta=e\hbar/m''c,\quad(3)$$

and m', m'', and Δm are functions of the relevant effective masses. These functions depend upon the geometry of the experiment and the shape of the electronic constant energy surface in momentum space for the crystal under investigation. E_0 is the energy at this surface measured from the bottom of the relevant zone in the case of electrons (or from the top in the case of holes) and is given by a quadratic function of the momenta. The first summation sign in Eq. (1) is included in order to account for the existence of several ellipsoidal surfaces characterized by different parameters and giving rise to beats. As will be borne out by the experimental data, it is possible to account almost completely for the observed oscillatory terms in arsenic by the introduction of four ellipsoids. At this point it is convenient to write the pertinent equations for these ellipsoids, postponing a discussion of their applicability to a later section.

1. Long-Period Oscillations

The long-period oscillations in arsenic will be interpreted in terms of a single ellipsoid of the form

$$E_{0l}=\frac{p_x^2+p_y^2}{2m_\perp}+\frac{p_z^2}{2m_{\parallel}},\quad(4)$$

where p_x, p_y, and p_z are the components of momentum parallel respectively to the binary axis, the bisectrix axis, and the trigional axis. $m_\perp$ and $m_{\parallel}$ are the effective electronic masses perpendicular and parallel respectively to the trigonal axis, and the subscript l refers to the long-period term.

$$m_l'=m_\perp(m_{\parallel})^{\frac{1}{2}},\quad(5)$$

$$(\Delta m)_l=m_\perp-m_{\parallel},\quad(6)$$

$$\beta_l=\frac{e\hbar}{cm_\perp(m_{\parallel})^{\frac{1}{2}}}(m_\perp\sin^2\phi+m_{\parallel}\cos^2\phi)^{\frac{1}{2}},\quad(7)$$

where ϕ is the angle between the trigonal axis and the magnetic field.

2. Short-Period Oscillations

The three-ellipsoid scheme proposed by Shoenberg for bismuth and antimony is appropriate, and the pertinent equations are copied below with only slight changes in notation.

$$2m_0E_{0s}=\alpha_1p_x^2+\alpha_2p_y^2+\alpha_3p_z^2+2\alpha_4p_yp_z,\quad(8)$$

and in addition the two ellipsoids derived from this one by rotations of $\pm\frac{2}{3}\pi$ about the p_z axis. The subscript s refers to the short-period oscillations, m_0 is the free-electron mass, and

$$\alpha_1=\frac{m_0}{m_1},\quad\alpha_2=\frac{m_0m_3}{m_2m_3-m_4^2},\quad\alpha_3=\frac{m_0m_2}{m_2m_3-m_4^2},$$

$$\alpha_4=\frac{m_0m_4}{m_2m_3-m_4^2}.$$

These ellipsoids lead to three periodic terms in Eq. (1) which, for the modes of measurement indicated, have the following values for β_s and $(\Delta m)_s$ provided H is in a horizontal plane and ϕ is the angle between the trigonal axis and the field.

(a) Binary axis vertical, trigonal axis horizontal

$$\beta_1=\lambda(m_3\cos^2\phi+m_2\sin^2\phi+2m_4\sin\phi\cos\phi)^{\frac{1}{2}},$$
$$\beta_2=\beta_3=\lambda(m_3\cos^2\phi+\tfrac{1}{4}(3m_1+m_2)\sin^2\phi-m_4\sin\phi\cos\phi)^{\frac{1}{2}},\quad(9)$$

$$(\Delta m)_1\sin\phi\cos\phi=\tfrac{1}{2}(m_2-m_3)\sin2\phi+m_4\cos2\phi,$$
$$(\Delta m)_2\sin\phi\cos\phi=(\Delta m)_3\sin\phi\cos\phi=\tfrac{1}{2}(\tfrac{3}{4}m_1+\tfrac{1}{4}m_2-m_3)\sin2\phi-\tfrac{1}{2}m_4\cos2\phi.\quad(10)$$

It should be noted that for this mode of measurement, ϕ and $\pi-\phi$ are not equivalent. As in Shoenberg's work, the sense of ϕ has been so chosen that ϕ increases from zero as the field turns away from the trigonal axis (0001) into the acute-angled sector between (0001) and $(10\bar{1}1)$.

(b) Binary and trigonal axes horizontal

$$\beta_1=\lambda(m_3\cos^2\phi+m_1\sin^2\phi)^{\frac{1}{2}}$$
$$\beta_2,\beta_3=\lambda[m_3\cos^2\phi+\tfrac{1}{4}(m_1+3m_2)\sin^2\phi\pm\sqrt{3}m_4\sin\phi\cos\phi]^{\frac{1}{2}},\quad(11)$$

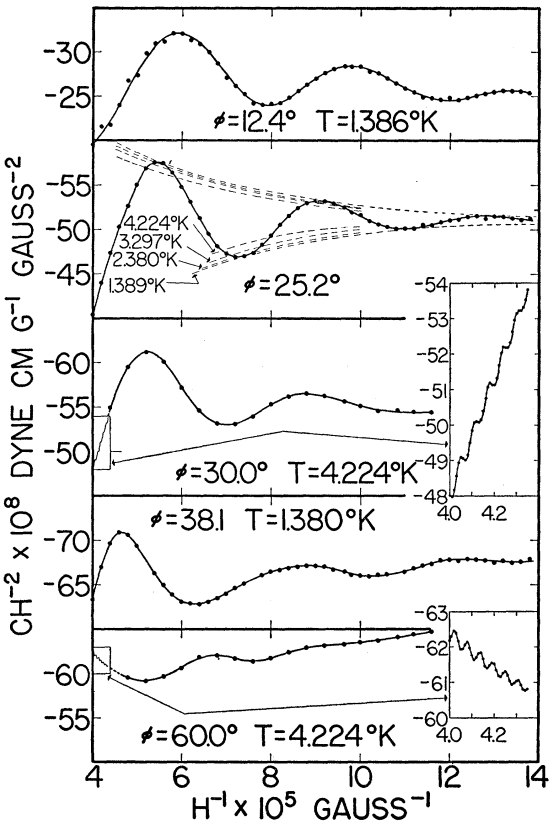

FIG. 1. As 1 (impure). CH^{-2}, which is proportional to the magnetic anisotropy $\Delta\chi$, *versus* H^{-1} for mode (*b*), binary and trigonal axes horizontal. ϕ is the angle between the trigonal axis and H. The short-period oscillations were present in general but are not plotted in detail in all cases.

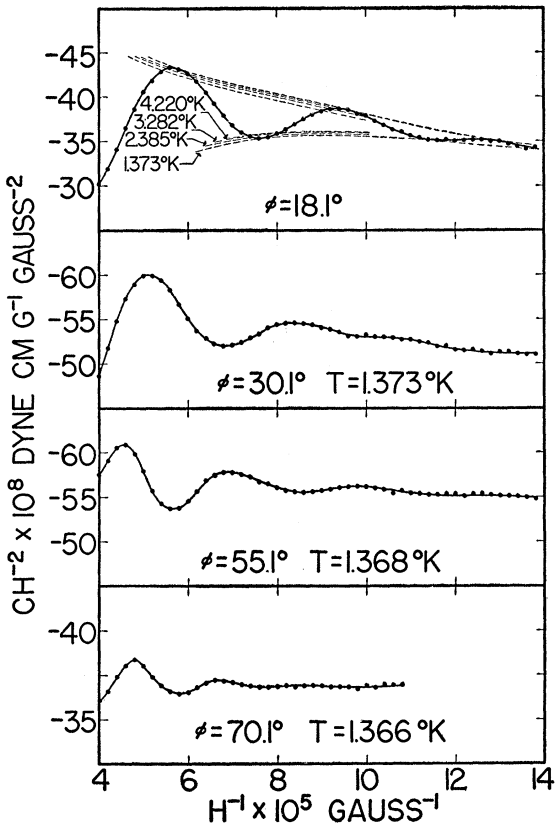

FIG. 2. As 1 (impure). CH^{-2} *versus* H^{-1} for mode (*a*), binary axis vertical, trigonal axis horizontal. Though not indicated, the short-period oscillations were present in general.

$$(\Delta m)_1 \sin\phi\cos\phi=\tfrac{1}{2}(m_1-m_3)\sin 2\phi,$$

$$(\Delta m)_2 \sin\phi\cos\phi,\ (\Delta m)_3 \sin\phi\cos\phi = \tfrac{1}{2}(\tfrac{1}{4}m_1+\tfrac{3}{4}m_2-m_3)\sin 2\phi \pm \tfrac{1}{2}\sqrt{3}m_4\cos 2\phi. \quad (12)$$

In both (*a*) and (*b*) above,

$$\lambda=\frac{e\hbar}{c[m_1(m_2m_3-m_4^2)]^{\frac{1}{3}}}, \quad (13)$$

and the m' of Eq. (2) is given by

$$m'=[m_1(m_2m_3-m_4^2)]^{\frac{1}{3}}. \quad (14)$$

EXPERIMENTAL WORK

1. Torsion Balance Method

The torsion balance method (which is described in detail elsewhere[2,14]) was used to measure the couple C per unit mass in a vertical direction acting on the crystal in a homogeneous magnetic field. This couple is related to $\Delta\chi$ [as given by Eq. (1)] by the expression:

$$C=\Delta\chi H^2\sin\phi\cos\phi, \quad (15)$$

where H is the magnetic field strength and ϕ is the angle measured in a horizontal plane between a given crystallographic axis and the magnetic field. Three modes of measurement were employed in this investigation, (*a*) binary axis vertical, trigonal axis horizontal, (*b*) binary and trigonal axes horizontal, (*c*) trigonal axis vertical.

Angular displacements of the crystal never exceeded 1° and displacements of approximately 0.0005° were detectable. Values of ϕ were corrected for these displacements, and measurements of the short-period terms were carried out over small ranges of field in order to avoid complications arising from their sensitive orientation dependence. Absolute values of CH^{-2} may be in error by as great as 2 percent because of possible errors in balance calibration, but relative values should be accurate to about 0.2 percent at high fields.

Temperatures were determined by observation of the vapor pressure of the liquid helium bath with mercury and oil manometers used in conjunction with the Mond vapor pressure tables.[15]

2. Magnet

An Arthur D. Little electromagnet capable of rotation about a vertical axis supplied horizontal magnetic fields up to 25 kilogauss in strength. Pole pieces 5.75

[14] Ted G. Berlincourt, Phys. Rev. **88**, 242 (1952).

[15] H. van Dijk and D. Shoenberg, Nature **164**, 151 (1949).

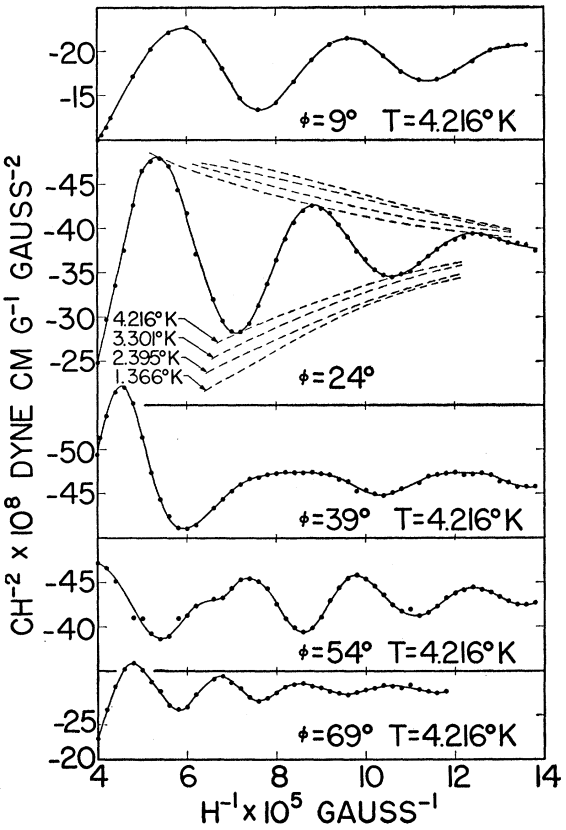

FIG. 3. As 2 (pure). CH^{-2} *versus* H^{-1} for mode (*b*), binary and trigonal axes horizontal. Note the beats for $\phi=39°$ and $\phi=54°$. The short-period oscillations were present in general.

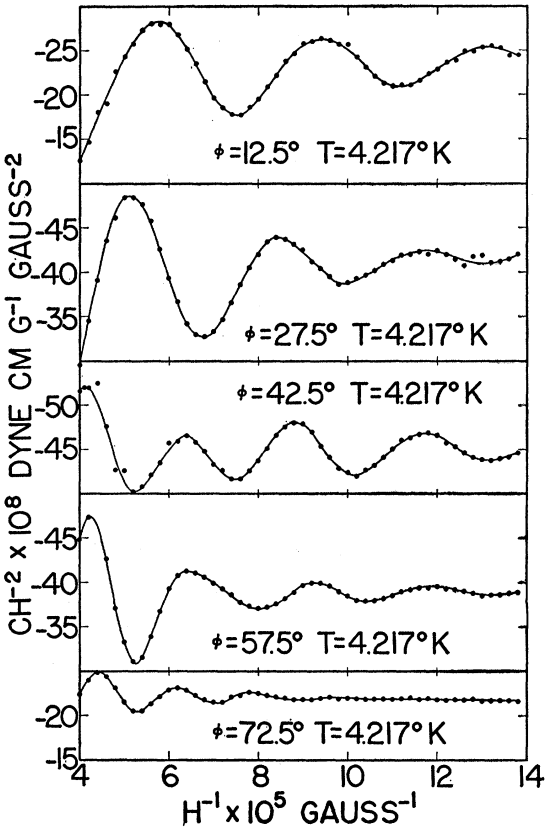

FIG. 4. As 2 (pure). CH^{-2} *versus* H^{-1} for mode (*a*), binary axis vertical, trigonal axis horizontal. Note the beats for $\phi=42.5°$ and $\phi=57.5°$. The short-period oscillations were present in general.

inches in diameter and a gap of 1.75 inches assured field homogeneity to within a few gauss over the volume of the crystal. The magnet was calibrated with a nuclear fluxmeter to an accuracy of better than 0.02 percent, and time variations of the field were limited to less than 5 gauss during the course of a single measurement.

3. Arsenic Crystals

Two arsenic crystals were used in this investigation. The first crystal, As 1, (weighing 13.7 milligrams) was a well-formed hexagonal plate cleaved at a small connecting link from a large crystalline mass of Fisher A892 "Purified Arsenic." A spectrochemical analysis kindly carried out by S. Cress of this laboratory revealed the following impurities: 0.1 to 1 percent Sb, 0.01 to 0.1 percent Bi, 0.01 to 0.1 percent Si, 0.001 to 0.01 percent, Cu, 0.001 to 0.01 percent Pb, and traces of Mg. The second crystal, As 2, (weighing 14.0 milligrams) was grown from the vapor with Johnson Matthey and Company, JM 640, Laboratory No. 6126 very high-purity arsenic. The spectroscopic report listed faintly visible lines from Ag, Cu, Mg, and Si.

Difficulties were anticipated in growing a crystal because of the many allotropic modifications of arsenic and the fact that it melts only at relatively high pressures and temperatures (see Mellor[16]). However, since it sublimes readily at moderate temperatures, growth from the vapor is feasible.[17] The method finally adopted will be described in some detail.

A simple furnace was constructed in the following way: A slot $\frac{11}{32}$ inch wide, 5 inches long and open at one end was cut in a $\frac{3}{8}$-inch thick slab of transite, and along both sides of the slot small holes were drilled 3 mm apart and 1.5 mm from the edge. Nichrome heater wire was threaded through these holes in spiral fashion. This piece was then placed on a 1-inch thick transite slab, and two small $\frac{3}{8}$-inch thick transite blocks were placed on top, each covering nearly half the length of the slot leaving a gap of about $\frac{1}{4}$ inch at the center. The nichrome wires were spread apart slightly at this gap to provide a "cool spot." Roughly 20 milligrams of arsenic were sealed under high vacuum into a 7-mm o.d. quartz tube about 3 inches long, which was in turn placed into the furnace slot. Heat was supplied until all of the arsenic was vaporized. A crystal was then nucleated by touching the quartz tube at the "cool spot" with a

[16] J. W. Mellor, *A Comprehensive Treatise on Inorganic and Theoretical Chemistry* (Longmans, Green and Company, London, 1929), Vol. 9, p. 16.

[17] McLennan, Niven, and Wilhelm, Phil. Mag. **6**, 666 (1928).

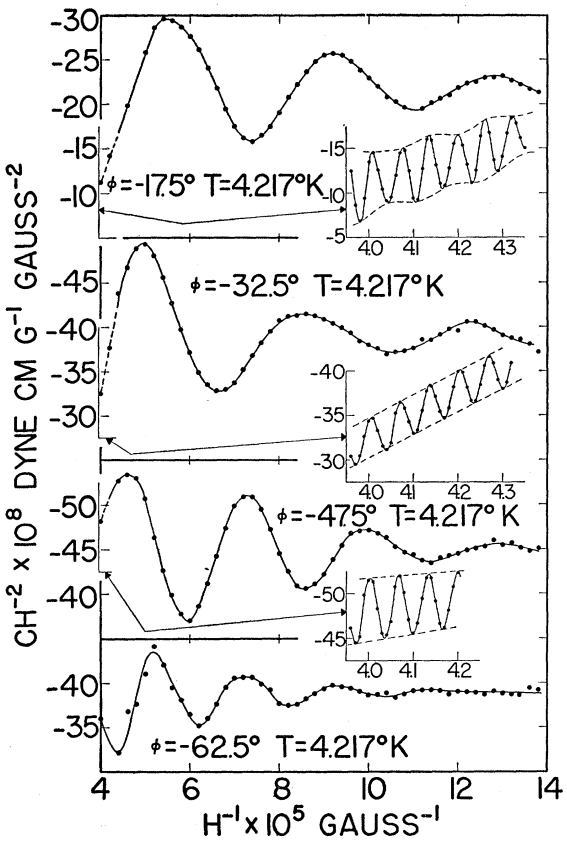

FIG. 5. As 2 (pure). CH^{-2} *versus* H^{-1} for mode (*a*), binary axis vertical, trigonal axis horizontal. Note the much larger amplitude for the short-period terms than was observed for As 1.

cool, sharp metal probe for a few seconds, and decreasing the power supplied to the furnace. The growth of the crystal was observed visually, the power being adjusted to obtain a suitable growth rate. In order to condense only the rhombohedral form of arsenic, it appeared to be necessary to vaporize all of the arsenic and then condense it at a relatively high temperature. Attempts to sublime a small part of a large quantity of arsenic from one region to a cooler region produced unwanted allotropic forms. It should be mentioned that the temperatures used often exceeded the softening point of Pyrex, which was used in place of quartz in early attempts.

As 2, produced in the above manner, displayed well-formed facets, and a goniometric investigated yielded reflections from the [0001], [01$\bar{1}$2], [10$\bar{1}$1], [20$\bar{2}$1], [10$\bar{1}$4] planes. All except the third of these forms were noted by Palache[18] in a natural arsenic crystal. Despite the fact that As 2 was the best crystal obtained, a Laue back-reflection x-ray picture taken after the magnetic measurements had been completed revealed considerable asterism. Since the crystal was attached to the torsion balance with Duco cement, strains were probably introduced via differential thermal expansion as the crystal was repeatedly cooled and warmed between room and helium temperatures. In fact it was noted by observation with a microscope that the quality of the facets deteriorated noticeably with successive runs.

[18] Charles Palache, Am. Mineralogist **26**, 709 (1941).

EXPERIMENTAL RESULTS

The features of the susceptibility oscillations in arsenic are illustrated in Figs. 1 through 6, where CH^{-2} which is directly proportional to $\Delta\chi$ [see Eq. (15)], is plotted against reciprocal field for the indicated modes of measurement. The reciprocal of the magnetic field is chosen for the abscissa in order to illustrate the periodicity in H^{-1} in agreement with Eq. (1). CH^{-2} is plotted as negative in all cases to indicate that $(\chi_{\parallel}-\chi_{\perp})$ is negative where $\chi_{\parallel}$ and $\chi_{\perp}$ are the components of susceptibility parallel and perpendicular respectively to the trigonal axis. Rather complete data for the long-period oscillations are included because of the presence of some unexplained features to be discussed later. Note the greater amplitude of the oscillations in As 2 in keeping with its higher purity.

In general, CH^{-2} is made up of a steady portion, plus a long-period term, plus three short-period terms, although usually only one short-period term is strong enough to be measured. For some orientations and at low fields the short-period terms were so weak that they could be ignored in taking the long-period term data. However, at high fields, points which determine the long-period curves were taken as the mean of the short-period oscillations over small intervals of field. It should be remembered that Figs. 1 through 5 are in most parts schematic in that the short-period terms were usually present. They were not traced out in detail over the entire range of fields as this procedure would have been prohibitively time-consuming. Note the presence of beats in the blow-up of the short-period

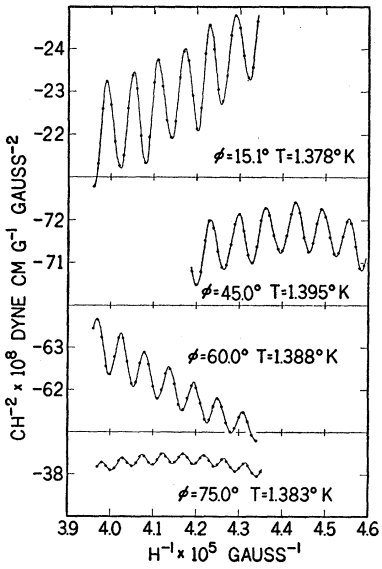

Fig. 6. As 1 (impure). CH^{-2} *versus* H^{-1} for mode (*b*), binary and trigonal axes horizontal. The shift of the mean of the short-period term arises from the long-period term illustrated in Figs. 1 through 5.

oscillations for $\phi=-17.5°$ in Fig. 5 indicating the existence of two short-period terms.

ANALYSIS AND EVALUATION OF PARAMETERS

1. The One Ellipsoid Scheme and the Long-Period Oscillations

Inspection of Eq. (1) reveals that the period of the susceptibility oscillations in reciprocal field is given by β/E_0. In order to deduce this parameter for the long-period term, envelope curves were drawn, and the mean of the oscillations was ascertained in each case. Then values of reciprocal field at which maxima, minima, and crossover points (or zeros of the sine function) occur were plotted against odd, even, and half-integers respectively as in Figs. 7 and 8. Values for β_l/E_{0l} were deduced from the slopes of the linear plots and are listed together with the corresponding amplitudes in Table I for the various orientations and modes of measurement.

At some orientations, as illustrated by the dashed lines, beats were present, and insufficient information was obtainable to permit determinations of the periods of the components. The presence of beats could indicate the inadequacy of the one ellipsoid scheme as outlined in the first section for the long period term, or the existence of small inclusions of different orientation in the crystals (even though not detected by the x-ray examination), or possibly both.

In any event, a test of the fit of the available experimental data to the one ellipsoid scheme was accomplished by plotting the square of the period against $\cos^2\phi$ for the (a) and (b) modes of measurement. If Eq. (7) is applicable, a straight line should be obtained with points for both modes falling on the same line. Such plots appear for the two crystals in Figs. 9 and 10. Evidently the one-ellipsoid scheme is a fair approximation. Note from Figs. 9 and 10 that the impure crystal, As 1, exhibited periods noticeably different from the pure crystal and far exceeding any difference attributable to the possible orientation errors of $\pm 2°$.

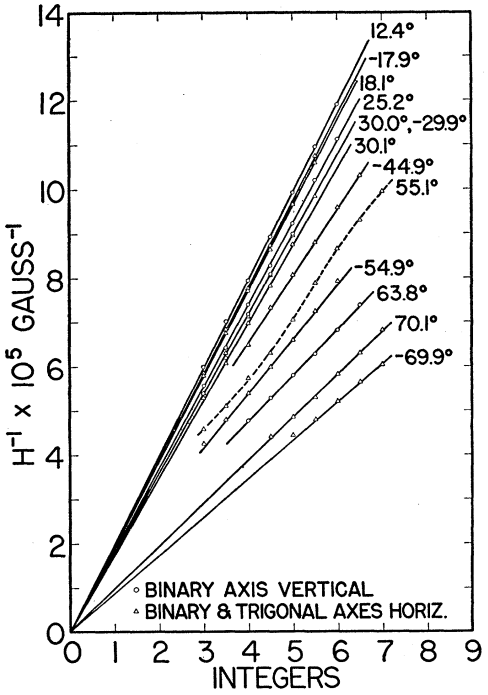

FIG. 7. As 1 (impure). Values of H^{-1} at which maxima, minima, and crossover points occur for the long period oscillations plotted against odd, even, and half integers respectively. Periods are calculated from the slopes of these lines and the phase is determined from the intercept on the integer axis.

TABLE I. Summary of data on the long-period term in arsenic.[a]

ϕ	$(\beta_l/E_{0l})\times10^5$	$a_l\times10^8$	$\beta_l\times10^{19}$	$E_{0l}\times10^{14}$	x_l	T
As 1, binary and trigonal axes horizontal					20 September 1954	
30.0	3.59	1.85			7.3	4.224
60.0	2.24	0.55				4.224
As 1, binary and trigonal axes horizontal					20 October 1954	
12.4	4.00	3.04			5.9	1.386
25.2	3.73	2.16				4.224
25.2	3.73	2.75	5.28	1.42		3.297
25.2	3.73	3.05				2.380
25.2	3.73	3.27			7.8	1.389
38.1	beats					1.380
51.0	beats					1.377
63.8	2.10	0.58				1.373
76.7	1.31	(0.1)				1.368
As 1, binary axis vertical					2 November 1954	
18.1	3.86	1.80				4.220
18.1	3.86	1.97	5.57	1.44		3.282
18.1	3.86	2.24				2.385
18.1	3.86	2.38			8.2	1.373
30.1	3.51	1.20				1.373
45.1	beats					1.372
55.1	beats					1.368
70.1	1.89	(0.2)				1.366
−17.9	3.89	2.58			7.1	1.363
−29.9	3.59	1.93			8.9	1.349
−44.9	2.99	1.63				1.357
−54.9	2.47	0.88				1.356
−69.9	1.73	(0.2)				1.342
As 2, binary and trigonal axes horizontal					17 January 1955	
9.0	3.74	4.18			3.0	4.216
9.0	3.74	4.78	5.90	1.58		3.301
9.0	3.74	5.42				2.403
9.0	3.74	5.92				1.380
24.0	3.50	6.86			4.5	4.216
24.0	3.50	7.98	5.64	1.59+		3.301
24.0	3.50	9.10				2.395
24.0	3.50	10.15				1.366
39.0	beats					4.216
54.0	2.48	(3.5)				4.216
69.0	1.86	1.00			2.2	4.216
As 2, binary axis vertical					24 January 1955	
12.5	3.68	4.35			3.2	4.217
27.5	3.30	4.45				4.217
42.5	beats					4.217
57.5	beats					4.217
72.5	1.80	0.47			3.6	4.217
−17.5	3.60	5.17			3.9	4.217
−32.5	3.30	3.87			5.3	4.217
−47.5	2.70	5.14			3.6	4.217
−62.5	2.14	1.42			4.5	4.217

[a] ϕ is the angle in degrees between the trigonal axis and the magnetic field; β_l/E_{0l} is in gauss^{-1}; a_l is the amplitude of the oscillations of CH^{-2} in dyne cm g^{-1} gauss^{-2} for $H^{-1}=8\times10^{-5}$; β_l is in erg gauss^{-1}; E_{0l} is in erg; x_l is in °K; T is in °K; less accurate values are indicated by parentheses.

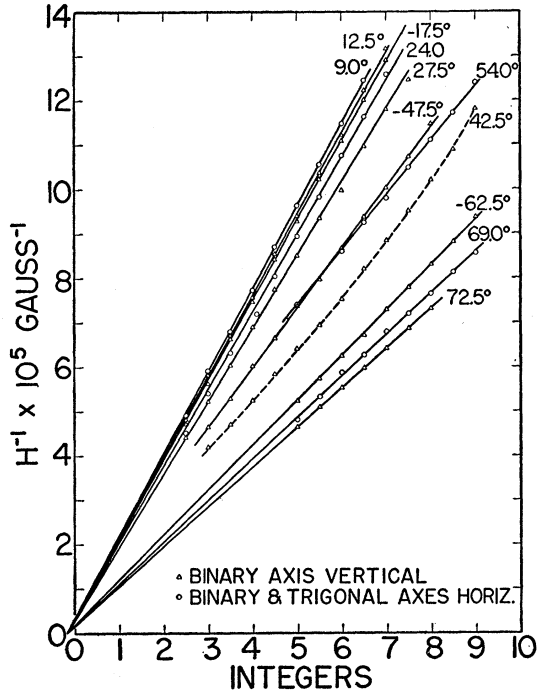

FIG. 8. As 2 (pure). Values of H^{-1} at which maxima, minima, and crossover points occur for the long-period oscillations plotted against odd, even, and half integers, respectively.

Additional support for the one-ellipsoid approximation, which predicts isotropy in the plane perpendicular to the trigonal axis, was obtained from measurements performed on both crystals with the trigonal axis vertical. These measurements yielded only very weak oscillations, too weak to analyze with any certainty, although the evidence suggested terms having periods of approximately 0.85×10^{-5} gauss^{-1} in As 2.

The phase of the long-period oscillations is also of interest and can be obtained from the intercepts on the integer axis of those plots in Figs. 7 and 8 for which an extrapolation to infinite field appears justified. For As 1, the observed phase $\delta=0.50\pi$ and for As 2, $\delta=0.31\pi$ whereas the theoretical phase as given in Eq. (1) is $\delta=-\pi/4$.

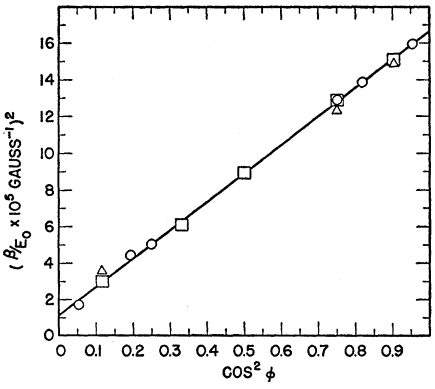

FIG. 9. As 1 (impure). The square of the period for the long-period term *versus* the square of the cosine of the angle ϕ between the trigonal axis and H. The circles correspond to measurement mode (b), the triangles correspond to mode (a) with ϕ positive, and the squares correspond to mode (a) with ϕ negative.

2. The Three-Ellipsoid Scheme and the Short-Period Oscillations

In determining periods for the short-period terms, a process similar to that described in the foregoing was adopted except that only crossover points were plotted against integers. Wherever beats occurred, the dominant period was taken as the mean period over several beat periods. The subordinate period could then be determined from the beat period. The values so obtained as well as the amplitude of the oscillations are tabulated in Table II.

In order to test the applicability of the bismuth-antimony type three-ellipsoid scheme to the short-period terms in arsenic, the square of the period was plotted against ϕ for measurement modes (a) and (b). Now according to Eqs. (9) and (11) the orientation

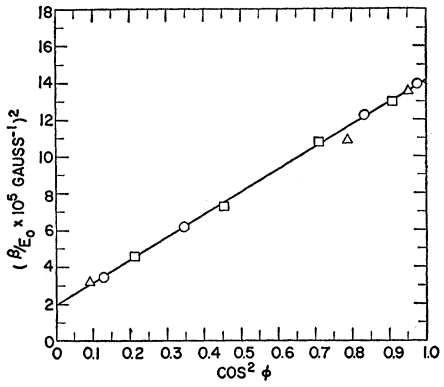

FIG. 10. As 2 (pure). The square of the period for the long-period term *versus* $\cos^2\phi$. The circles correspond to measurement mode (b), the triangles correspond to mode (a) with ϕ positive, and the squares correspond to mode (a) with ϕ negative.

dependence of the period for the ith short-period term should be of the form

$$(\beta_i/E_{0s})^2=f_i+g_i\sin(2\phi+\theta_i), \qquad (16)$$

where f_i and g_i involve the effective masses as well as E_{0s} and other constants, θ_i involves the effective masses only, and i runs from 1 to 3 for each measurement mode. Once any four of these parameters have been determined, the other 14 are fixed. By a method of successive approximations a self-consistent set of parameters was ascertained which gave a satisfactory fit to the experimental points, verifying the applicability of the three-ellipsoid scheme. The curves in Figs. 11 through 14 were drawn by using these parameters, and it should be pointed out that very slight modifications (of the order of one percent) of the parameters produce noticeably poorer fits to the data. Note again that

TABLE II. Summary of data on the short period terms in arsenic.[a]

ϕ	$(\beta_s/E_{0s})\times10^{7}$	$a_s\times10^{8}$	$\beta l\times10^{19}$	$E_{0s}\times10^{14}$	x_s	T
As 1, binary axis vertical					13 August 1953	
14.2	5.79	0.46				1.840
28.7	5.85	0.74				1.842
43.6	5.28	1.00				1.842
58.7	4.52	0.34				1.843
74.2	(3.9)	(0.05)				1.843
−2.7	5.44	0.38				4.224
−13.9	6.27	0.57				4.224
−28.4	6.73	0.56				4.224
−43.0	6.81	0.37				4.224
−58.3	6.27	0.72	(1.73)	(27.6)	(5.8)	4.224
−58.3	6.27	1.59			(6.6)	1.842
−73.7	5.34	0.21	(1.48)	(27.7)		4.224
−73.7	5.34	0.59				1.842
As 1, binary and trigonal axes horizontal					30 September 1954	
15.1	5.99	1.06				1.378
30.0	6.42	0.241				4.224
30.0	6.42	0.332	1.86	29.0		3.307
30.0	6.42	0.427				2.380
30.0	6.42	0.556				1.389
45.0	6.41	0.754				1.395
60.0	5.72	0.181				4.224
60.0	5.72	0.256	1.69	29.6		3.301
60.0	5.72	0.350				2.380
60.0	5.72	0.470				1.388
75.0	4.77	0.110				1.383
−15.0	6.17	0.361				1.379
−22.4	6.32					1.381
−29.9	6.42	0.425				1.384
−44.9	6.37	1.16				1.390
−52.4	6.09					1.391
−59.9	5.68	1.32				1.392
−67.4	5.36					1.392
−75.0	4.69	0.280				1.393
As 2, binary and trigonal axes horizontal					17 January 1955	
9.0	5.76	2.30				4.216
9.0	5.76	3.33	1.70	29.5		3.301
9.0	5.76	4.36				2.403
9.0	5.76	5.82				1.380
9.0	4.62	0.35				4.216
9.0	4.62	0.49				3.301
As 2, binary and trigonal axes horizontal January 17, 1955—*Continued*						
9.0	4.62	0.69				2.403
9.0	4.62	0.91				1.380
24.0	6.11	1.82				4.216
24.0	6.11	2.69	1.79	29.3		3.301
24.0	6.11	3.42				2.395
24.0	6.11	4.45				1.366
24.0	5.02	0.57				4.216
24.0	5.02	0.82				3.301
24.0	5.02	1.13				2.395
24.0	5.02	(1.70)				1.366
39.0	6.35	1.53				4.216
39.0	4.50	0.30				4.216
54.0	5.95	3.40				4.216
69.0	5.25	1.91				4.216
84.0	4.16	(0.4)				4.216
−15.0	5.80	4.00				4.216
−30.0	6.30	1.38				4.216
−45.0	6.29	2.37				4.216
−60.0	5.61	2.90				4.216
−75.0	4.92	(1.3)				4.216
As 2, binary axis vertical					24 January 1955	
7.5	5.52					4.217
12.5	5.53	(1.0)				4.217
18.0	3.81					4.217
35.0	5.60					4.217
42.5	5.60	1.43				4.217
50.0	5.37					4.217
57.5	4.85	(1.0)				4.217
65.0	4.23					4.217
72.5	3.80	0.10				4.217
80.0	3.47					4.217
−7.5	5.68					4.217
−17.5	6.21	3.17				4.217
−17.5	4.33	0.48				4.217
−25.0	6.59					4.217
−32.5	6.62	2.25				4.217
−47.5	6.57	3.27				4.217
−55.0	6.40					4.217
−70.0	5.57					4.217
−77.5	4.77	1.03				4.217
−85.0	4.36					4.217

[a] ϕ is the angle in degrees between the trigonal axis and the magnetic field; β_s/E_{0s} is in gauss^{-1}; a_s is the amplitude of the oscillations of CH^{-2} in dyne cm g^{-1} gauss^{-2} for $H^{-1}=4.1\times10^{-5}$; β_s is in erg gauss^{-1}; x_s is in °K; T is in °K; less accurate values are indicated by parentheses; wherever no entry appears under a_s, oscillations were counted.

small differences exist between the results for As 1 and As 2, the impure crystal again exhibiting the longer periods. No determination of the phases of the short-period oscillations was possible since extrapolation to infinite field could not be made with any certainty.

3. Effective Masses and Degeneracy Energies

Provided Eq. (1) is valid, a plot of

$$\log_e\{aT^{-1}[1-\exp(-4\pi^2kT/\beta H)]\}$$

(where a is the amplitude of the oscillations in CH^{-2} for a given term) against T for fixed H should yield a straight line of slope $-2\pi^2k/\beta H$. Thus, a first approximation to β may be obtained from the slope of a plot of $\log_e(aT^{-1})$ against T. This value of β may then be used in a plot of

$$\log_e\{aT^{-1}[1-\exp(-4\pi^2kT/\beta H)]\}$$

against T, yielding a second approximation to β. This process may be repeated until a value of β of the desired accuracy is obtained. Values of β so derived appear in Tables I and II, and examples (using $\log_{10}$) of such final plots appear in Fig. 15. The theoretical form of the temperature dependence of amplitude is verified by the linearity of these plots. [Incidentally, the harmonics appearing in Eq. (1) were not important at the fields and temperatures involved in these plots.]

Once β had been determined, E_0 was determined from the period β/E_0. Values for both long and short period terms in both crystals appear in Tables I and II.

Comparisons of Eq. (7) with Figs. 9 and 10, Eq. (9) with Figs. 11 and 12, and Eq. (11) with Figs. 13 and 14 permitted evaluation of the pertinent electronic effective masses. These are listed together with the best values for E_0, Table III. (The values for m_{11}/m_0 in parentheses were derived by another method discussed in a later section.)

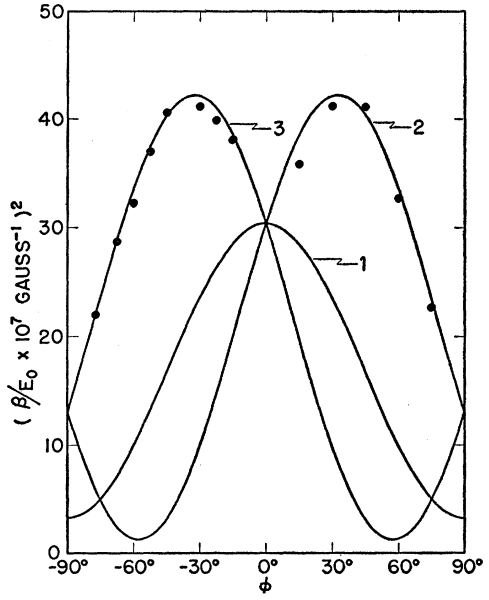

FIG. 11. As 1 (impure). Square of the period for the short-period terms *versus* ϕ for mode (*b*), binary and trigonal axes horizontal.

4. Field Dependence of Amplitude

According to a modification of Landau's theory by Dingle,[19] broadening of the electronic energy levels resulting from the presence of impurities has the effect of reducing the amplitude of each term in the summation over p in Eq. (1) by a factor

$$\exp(-2\pi^2 pkx/\beta H),$$

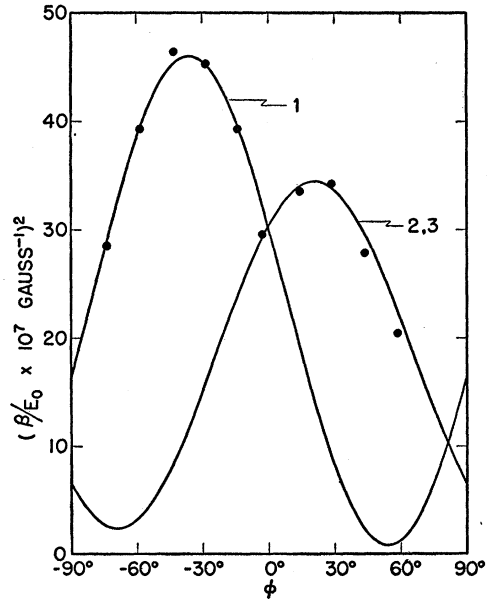

FIG. 12. As 1 (impure). Square of the period for the short-period terms *versus* ϕ for mode (*a*), binary axis vertical, trigonal axis horizontal.

[19] R. B. Dingle, Proc. Roy. Soc. (London) **A211**, 517 (1952).

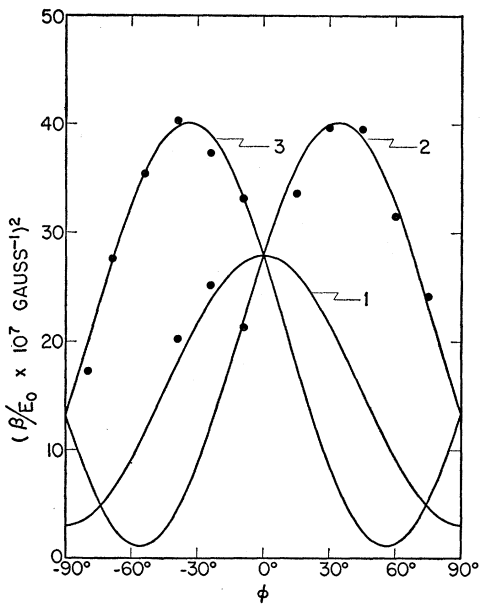

FIG. 13. As 2 (pure). Square of the period for the short-period terms *versus* ϕ for mode (*b*), binary and trigonal axes horizontal. Where two points occur for one angle, beats were observed.

where x has the dimension of temperature and is related to the collision time τ by the expression

$$x=h/2\pi^2 k\tau. \tag{17}$$

It can be shown that if Eq. (1) is valid, $T+x$ is given by the product of $-\beta/2\pi^2 k$ and the slope of the straight line obtained when $\log_e\{aH^{\frac{1}{2}}[1-\exp(-4\pi^2 kT/\beta H)]\}$ is plotted against H^{-1} for fixed T. Several such plots

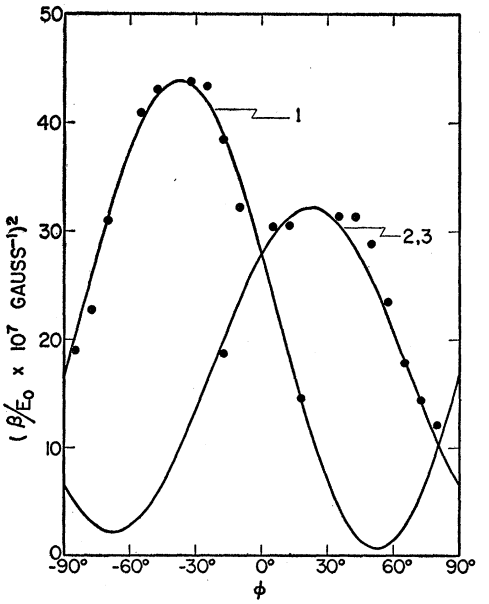

FIG. 14. As 2 (pure). Square of the period for the short-period terms *versus* ϕ for mode (*a*), binary axis vertical, trigonal axis horizontal.

appear in Fig. 16 for the long-period term in As 2. The linearity of these plots verifies the theoretical field dependence of amplitude. Where the plots are nonlinear, it appears that the beats already mentioned prohibit a comparison between theory and experiment. For the indicated fields and temperatures the harmonics were again negligible, although at the lowest temperatures and highest fields their presence was easily recognizable in the long-period term in As 2.

Values of x, derived from plots such as appear in Fig. 16, are tabulated in Tables I and II, and the large magnitudes are in keeping with the known relatively poor crystal quality. The short-period term values are not very reliable because of the relatively small range of fields investigated. In general, x was greater in As 1 as might be expected because of its greater impurity content. Although the dependence of x_l upon ϕ is somewhat irregular, the data for As 2 suggest that x_l increases as ϕ is increased from zero, reaches a maximum value at about $\pi/6$, and then decreases to roughly its initial value as ϕ approaches $\pi/2$. Croft, Love, and Nix[20] have proposed a mechanism which would give rise to an orientation-dependent x, but the scatter of the present data does not justify a detailed interpretation in terms of this mechanism.

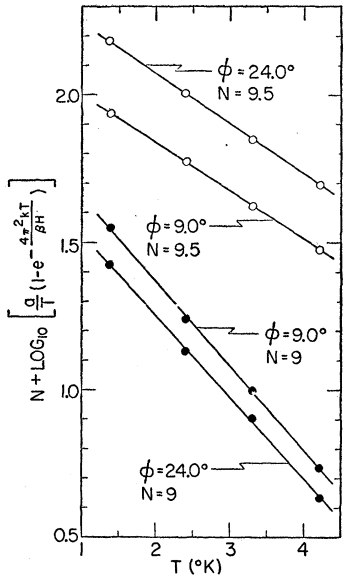

FIG. 15. As 2 (pure). Temperature dependence of the amplitude of the de Haas-van Alphen oscillations for mode (b), binary and trigonal axes horizontal. The open circles correspond to the long-period oscillations, and the solid circles correspond to the short-period terms. Values of β are derived from the slopes of such plots.

5. Absolute Amplitude, Steady Anisotropy, and Number of Electrons

If the degeneracy energy, the electronic effective masses, and x are known for a given de Haas-van Alphen term, the theoretical amplitude can be calculated using Eq. (1) together with Dingle's impurity damping factor. Such a calculation was carried out for the long period term for mode (b) (binary and trigonal axes horizontal) for As 1 with $\phi=25.2°$, $H^{-1}=9\times10^{-5}$, and $T=1.389°$K, and for As 2 with $\phi=24.0°$, $H^{-1}=9\times10^{-5}$, and $T=4.216°$K. The observed amplitudes exceeded the calculated amplitudes in As 1 and As 2 by factors of 28 and 29 respectively. Similar calculations for the short-period term, using long-period term values for x (which is probably not too bad an approximation),

TABLE III. The de Haas-van Alphen parameters for arsenic.[a]

	As 1 (impure)	As 2 (pure)
E_{0l} (erg)	1.43×10^{-14}	1.59×10^{-14}
$m_\perp/m_0$	3.18×10^{-2}	3.10×10^{-2}
$m_{\parallel}/m_0$	0.468 (4.4×10^{2})	0.231 (1.4×10^{2})
n_l per atom	1.8×10^{-6} (6.4×10^{-5})	1.5×10^{-6} (3.6×10^{-5})
δ (radians)	$0.50\,\pi$	$0.31\,\pi$
E_{0s} (erg)	29.3×10^{-14}	29.4×10^{-14}
m_1/m_0	0.187	0.193
m_2/m_0	0.956	1.07
m_3/m_0	1.77	1.78
m_4/m_0	−1.25	−1.33
n_s per atom	1.2×10^{-3}	1.2×10^{-3}

[a] Except where double entries appear, the probable errors are of the order of a few percent. The values for $m_{\parallel}/m_0$ appearing in parentheses were derived from the absolute amplitude of the long-period oscillations. The large discrepancy between these values and the ones obtained as described in part 3 of "Analysis and Evaluation of Parameters" is discussed in the text. n_s refers to each of the three short-period ellipsoids.

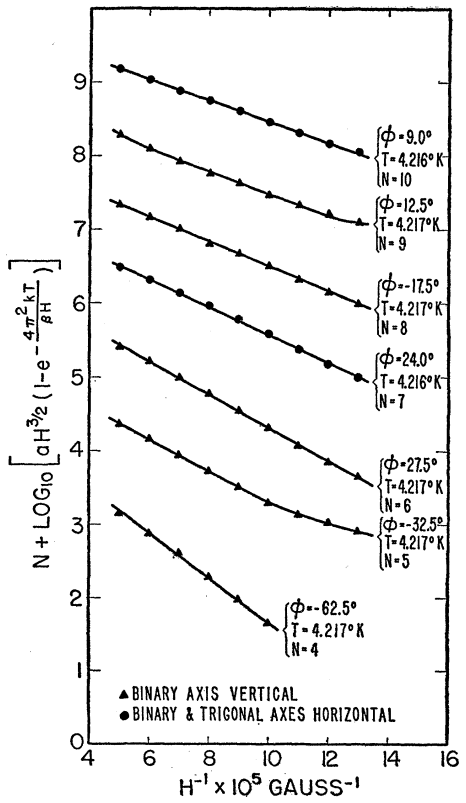

FIG. 16. As 2 (pure). Field dependence of the amplitude of the long-period oscillations. Values of the amplitude damping parameter x are derived from the slopes of such plots if linear.

[20] Croft, Love, and Nix, Phys. Rev. 95, 1403 (1954).

TABLE IV. Steady magnetic anisotropy of arsenic.

	$(\chi_{\parallel}-\chi_{\perp})_{\text{steady}}\times 10^6$ (emu)	
T (°K)	As 1 (impure)	As 2 (pure)
300	−0.82	−0.54
77	−1.2	−0.80
4.2	−1.3	−0.91

yielded agreement between theory and experiment to within a factor of two in several cases. This is quite satisfactory agreement in view of the uncertainties in the use of the long-period term x. On the other hand, the discrepancy in the long-period case is not easily accounted for. Examination of the parameters involved in the calculations reveals $m_{\parallel}$ (derived from the $\cos^2\phi=0$ intercept in Figs. 9 and 10) as the least accurately determined. Adjustment of $m_{\parallel}$ by an amount sufficient to bring experimental and calculated amplitudes into accord requires the values for $m_{\parallel}/m_0$ appearing in parentheses in Table III. Further possible support for these larger masses exists in that they bring the calculated steady anisotropy [first term in Eq. (1)] into accord (within 10 percent) with the experimentally observed values listed in Table IV. However, even though the effect of the short-period term electrons was also taken into account in this comparison, other conduction electrons (whose de Haas-van Alphen oscillations are not observable under present experimental conditions) may exist in arsenic, making such a comparison only speculative. Furthermore, it appears unlikely that the $\cos^2\phi=0$ intercepts in Figs. 9 and 10 could be so much in error. It is more likely that the answer lies in the inadequacy of the one-ellipsoid scheme or in the theory itself.

The number of long- and short-period electrons per atom listed in Table III were calculated from the following expressions.

$$n_l=\frac{8\pi}{3h^3}\frac{V}{N}m_{\perp}m_{\parallel}^{\frac{1}{2}}(2E_{0l})^{\frac{3}{2}}, \tag{18}$$

$$n_s=\frac{8\pi}{3h^3}\frac{V}{N}[m_1(m_2m_3-m_4^2)]^{\frac{1}{2}}(2E_{0s})^{\frac{3}{2}}, \tag{19}$$

where V is the atomic volume and N is Avogadro's number. The values in parentheses were calculated using the values for $m_{\parallel}/m_0$ in parentheses.

CONCLUDING REMARKS

The forms of the observed temperature and field dependences of the amplitude of the de Haas-van Alphen oscillations in arsenic are in good accord with theory. However, the phase of the long-period oscillations is at wide variance with theory as is typical in other crystals. In this connection it is of interest to note that As 1, which exhibited a greater maximum period than did As 2, also exhibited the greater phase. Furthermore, in zinc[21] (which displays a temperature-dependent period), as the maximum period increases the phase increases. A generalization on this observation may, however, be premature.

The short-period oscillations in arsenic can be accounted for quite satisfactorily by a three-ellipsoid constant-energy surface scheme. On the other hand, the one-ellipsoid scheme proposed as an approximation for the long-period term is less satisfactory because of the unexplained beats, the long-period oscillations observed (though weak) with the trigonal axis vertical, and the discrepancy between observed and calculated amplitudes. It may be mentioned that the values for $m_{\perp}$ and E_{0l} in arsenic are quite comparable with the corresponding values for graphite, and that in order to account for the large amplitude of the oscillations in graphite, Shoenberg[2] found it necessary to attribute to $m_{\parallel}$ a value of a few hundred free-electron masses as is necessary in the case of arsenic.

In order to obtain an explanation for the beats in the long-period term in arsenic, it is likely that better crystals would be necessary with correspondingly larger amplitude, thus facilitating measurements over a greater range of fields and with the trigonal axis vertical. It appears doubtful that the observed beats arise from small differently-oriented regions in the crystals in view of the similarity of the results for the two crystals used in this investigation. However, this possibility cannot be ruled out with certainty.

ACKNOWLEDGMENTS

It is a pleasure to acknowledge the generous assistance of Mr. Ralph Anonsen in the acquisition and reduction of data.

[21] Ted G. Berlincourt and M. C. Steele, Phys. Rev. **95**, 1421 (1954).